

Analysis of accretion disc structure and stability using open code for vertical structure

A. S. Tavleev,^{1,2*} G. V. Lipunova,^{1,3} and K. L. Malanchev^{1,4}

¹ Sternberg Astronomical Institute, Moscow M. V. Lomonosov State University, 13 Universitetski pr., 119234, Moscow, Russia

² Institut für Astronomie und Astrophysik, Kepler Center for Astro and Particle Physics, Universität Tübingen, Sand 1, 72076 Tübingen, Germany

³ Max-Planck-Institut für Radioastronomie, Auf dem Hügel 69, 53121 Bonn, Germany

⁴ Department of Astronomy, University of Illinois at Urbana-Champaign, 1002 W. Green St., IL 61801, USA

Accepted 2023 June 19. Received 2023 June 15; in original form 2022 December 6

ABSTRACT

Radial structure of accretion discs around compact objects is often described using analytic approximations which are derived from averaging or integrating vertical structure equations. For non-solar chemical composition, partial ionization, or for super-massive black holes, this approach is not accurate. Additionally, radial extension of ‘analytically-described’ disc zones is not evident in many cases. We calculate vertical structure of accretion discs around compact objects, with and without external irradiation, with radiative and convective energy transport taken into account. For this, we introduce a new open Python code, allowing different equations of state (EoS) and opacity laws, including tabular values. As a result, radial structure and stability ‘S-curves’ are calculated for specific disc parameters and chemical composition. In particular, based on more accurate power-law approximations for opacity in the disc, we supply new analytic formulas for the farthest regions of the hot disc around stellar-mass object. On calculating vertical structure of a self-irradiated disc, we calculate a self-consistent value of the irradiation parameter C_{irr} for stationary α -disc. We find that, for a fixed shape of the X-ray spectrum, C_{irr} depends weakly on the accretion rate but changes with radius, and the dependence is driven by the conditions in the photosphere and disc opening angle. The hot zone extent depends on the ratio between irradiating and intrinsic flux: corresponding relation for $T_{\text{irr, crit}}$ is obtained.

Key words: accretion, accretion discs – instabilities – X-rays: binaries

1 INTRODUCTION

Disc accretion is a common astrophysical phenomenon widely observed thanks to high efficiency of energy conversion to emission. Brightest sources of the X-ray sky are explained by accretion of matter on compact objects, and visibility of such sources allows us to investigate physics operating there. Many X-ray sources are found in binary systems where the matter flows from one component to another and accretion discs are formed.

The standard model of viscous accretion discs (Shakura 1972; Shakura & Sunyaev 1973) is based on the notion of the turbulent viscosity as a mechanism for the angular momentum transfer, allowing the matter, rotating around a central object, to move inwards and to emit gravitational energy converted to heat. Heat balance determines the vertical structure of the disc, that is, in the direction perpendicular to its symmetry plane. It is safe to assume that hydrostatic equilibrium holds in the vertical direction, meaning that the time to achieve the hydrostatic balance is shorter than other characteristic disc times. The thermal balance in the vertical direction occurs on a time-scale longer than a hydrostatic one, but faster than the disc evolves due to accretion rate variations. Thus, generally, the vertical disc structure could be studied separately from the radial one.

Considering accretion onto compact object of stellar masses, it is

commonly assumed that the standard model describes well the disc regions that emit mainly in the optical. In this context, the details of the disc vertical structure are important since they determine the brightness and spectra of those regions.

It has been known for some time that the vertical structure of accretion disc is subject to various instabilities. Thermal-viscous instability is believed to be a cause of outbursts occurring rather periodically in some sources with accretion discs. A model based on the instability has been developed in a number of works (e.g., Hōshi (1979); Smak (1982a); Meyer & Meyer-Hofmeister (1981, 1982); Faulkner et al. (1983); Papaloizou et al. (1983); Smak (1984)). Presently, it is referred to as the Disc Instability Model (or DIM, Hameury et al. 1998; Lasota 2001; Hameury 2020), see also Bagińska et al. (2021). Details of DIM depend not only on the disc vertical structure at different radii but on the radial energy transport as well. To some extent, using the local analysis alone, it is possible to study the scenario with thermal-viscous instability on a basis of so-called S-curves (Meyer & Meyer-Hofmeister 1981), or equilibrium curves. An S-curve is a graphically depicted sequence of solutions of the vertical-structure equations, obtained at a single disc radius, in the coordinates of accretion rate or effective temperature versus the surface density (see Fig. 8 below). The positive slope of an S-curve represents the thermally and viscously stable state of the disc, whereas the negative slope represents the unstable state.

In X-ray transients, burst evolution depends crucially on the self-irradiation of the disc: heating by central X-rays can change the local

* E-mail: tavleev@astro.uni-tuebingen.de

state of the outer disc and, thus, the viscosity there (Tuchman et al. 1990; Dubus et al. 2001). Vertical structure of a self-irradiated α -disc has been calculated by Tuchman et al. (1990); Dubus et al. (1999), who introduced a self-irradiation parameter. Self-consistent calculations of the vertical structure of irradiated discs have been performed by Mescheryakov et al. (2011) for fully ionized disc regions with opacity from the Opacity Project (Badnell et al. 2005).

In the current paper, we present results obtained with our new open Python code with modern values of opacity (Iglesias & Rogers 1993, 1996; Ferguson et al. 2005) and equations of state (Rogers & Nayfonov 2002)¹. The code calculates the vertical structure, S-curves, and radial profiles of optically thick accretion discs. We take into account X-ray irradiation by two methods and vertical transfer of energy by convection using an approach of the mixing-length theory. The code uses MESA package (Paxton et al. 2011) for interpolation and sewing of the opacity and EoS tables.

For un-irradiated discs, we analyse physical conditions in the discs for a wide range of parameters. We examine to what extent analytical approximations for opacity laws, and, consequently, for radial dependencies, can be satisfactorily used.

We analyse stability conditions for un-irradiated and self-irradiated discs. For self-irradiated discs, we also calculate the value of the self-irradiation parameter in the thermally stable disc parts, and analyse its dependence on the basic parameters of accretion disc.

In section 2, we present a system of equations of the vertical structure and boundary conditions, in particular, in the presence of external X-ray irradiation. The radial structure of the disc, resulting from solutions for vertical structure, is investigated in section 3. The irradiation parameter is considered there as well. In section 4, we construct and analyse S-curves. In section 5 we analyse and discuss the stability criterion of the irradiated disc. Summary is given in section 6. Appendix A reviews equations used in presence of external X-ray disc irradiation, while appendix B contains a brief description of the code. Appendix C provides several examples of vertical structures calculated by the new code.

2 MODELLING OF ACCRETION DISC VERTICAL STRUCTURE

The vertical structure of α -discs has been solved in a number of papers, including Smak (1984); Meyer & Meyer-Hofmeister (1982); Hameury et al. (1998); Lasota et al. (2008) where discs in X-ray transients were considered in particular. Note that they used previous values of opacity (Cox & Stewart 1969; Cox & Tabor 1976; Alexander 1975) and EoS (Fontaine et al. 1977). Ketsaris & Shakura (1998); Suleimanov et al. (2007); Malanchev et al. (2017) have solved the vertical structure with analytical opacity coefficient and equation of state, which allows obtaining analytical radial structure (see Sect. 3).

We use a cylindrical coordinate system (r, φ, z) , where z changes from 0 in the symmetry plane to the semi-thickness of disc z_0 on the disc surface. We consider geometrically thin ($z_0 \ll r$) Keplerian ($\omega = \omega_K = \sqrt{GM/r^3}$) stationary ($\partial/\partial t = 0$) optically thick ($\tau \gg 1$) accretion disc.

¹ Opacities of Iglesias & Rogers (1993, 1996) and Badnell et al. (2005) differs by up to 10% in area of typical disc parameters.

2.1 Basic equations

The vertical structure is described by the system of four ordinary differential equations (see e.g. Shakura et al. 2018), which follows from the mass, energy and momentum conservation laws. For moderate accretion rates and small temperature gradients along the radius, the energy balance is local. First we consider discs without external heating by irradiation.

$$\frac{dP}{dz} = -\rho \omega_K^2 z, \quad (1)$$

$$\frac{dQ}{dz} = \frac{3}{2} w_{r\varphi} \omega_K = \frac{3}{2} \omega_K \alpha P, \quad (2)$$

$$\frac{d \ln T}{d \ln P} \equiv \nabla = \begin{cases} \nabla_{\text{rad}}, & \nabla_{\text{rad}} \leq \nabla_{\text{ad}}, \\ \nabla_{\text{conv}}, & \nabla_{\text{rad}} \geq \nabla_{\text{ad}}, \end{cases} \quad (3)$$

$$\frac{d\Sigma}{dz} = -2\rho, \quad (4)$$

$$z \in [0, z_0].$$

Here $P = P_{\text{rad}} + P_{\text{gas}}$ is the total pressure, Q is the heating flux, which for an un-irradiated disc equals the viscous flux Q_{vis} , and T is the temperature. The mass coordinate $\Sigma(z)$ equals to zero at $z = 0$ and the surface density of the disc Σ_0 at $z = z_0$. The last part of (2) includes the α -prescription (Shakura & Sunyaev 1973), where the absolute value of the $r\varphi$ -component of tensor of viscous tensions $w_{r\varphi} = \alpha P$, and α is the turbulent parameter ($0 < \alpha < 1$).

If the energy is transported solely by radiation diffusion, equation (3) implies that

$$\nabla = \nabla_{\text{rad}} \equiv \frac{3\kappa_{\text{R}}}{4ac\omega_K^2 z} \frac{P}{T^4} Q, \quad (5)$$

where κ_{R} is the Rosseland opacity coefficient, $a = 4\sigma_{\text{SB}}/c$ is the radiation constant, c is the speed of light. Otherwise, if $\nabla_{\text{rad}} \geq \nabla_{\text{ad}}$, the convective motions start to transfer energy according to the Schwarzschild (1958) criterion. The corresponding temperature gradient ∇_{conv} can be calculated according to the mixing length theory (see Paczyński 1969; Kippenhahn et al. 2012; Hameury et al. 1998). Note that Malanchev & Shakura (2015) considered viscous energy generation in convective cells and found that it made convection energy transfer less efficient. The thermodynamic values, needed to calculate the temperature gradient, for example ∇_{ad} , are obtained from the eos module of the MESA code (Paxton et al. 2011).

In some cases, for the sake of comparison, we calculate the disc structure forcing $\nabla = \nabla_{\text{rad}}$ everywhere and call such models as ‘no convection’.

2.2 Equation of state and opacity law

System (1–4) should be supplemented by equation of state (EoS) and opacity law. They can be set both analytically or as tabular values. For analytical description, the ideal gas equation is adopted, while the opacity coefficient is approximated by a power-law function:

$$\rho = \frac{\mu P_{\text{gas}}}{\mathcal{R}T}, \quad \kappa_{\text{R}} = \kappa_0 \frac{\rho^\zeta}{T^\gamma}. \quad (6)$$

Here μ is the molecular weight and κ_0 is the dimension constant, which we give below in CGS units. For opacity, we consider the following options:

- the Kramers law for bound-bound and free-free transitions with $\zeta = 1, \gamma = 7/2$. For the solar chemical composition $\kappa_0 = 5 \cdot 10^{24}$ (Frank et al. 2002).

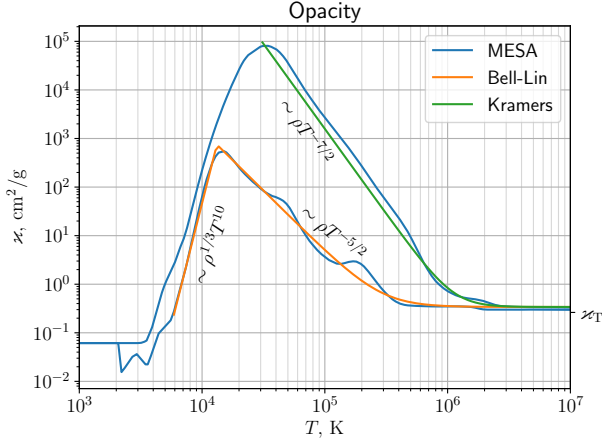


Figure 1. Rosseland opacity coefficient, tabular and analytical, for solar chemical composition and for two bulk densities, $\rho = 10^{-4}$ and 10^{-7} g cm $^{-3}$ (the upper and lower lines, respectively). The blue lines show interpolation of the tabular values (see Sect. 2.2). Orange and green lines show Kramers (Frank et al. 2002) and Bell & Lin (1994) power-law approximations.

- Two approximations by Bell & Lin (1994) to opacity produced by bound-free and free-free transitions with $\kappa_0 = 1.5 \cdot 10^{20}$, $\zeta = 1$, $\gamma = 5/2$ and scattering off hydrogen atoms with $\kappa_0 = 1 \cdot 10^{-36}$, $\zeta = 1/3$, $\gamma = -10$.

At $T \gtrsim 10^6$ K the opacity is dominated by the Thomson electron scattering, i.e. $\kappa_R = 0.34$ cm 2 g $^{-1}$.

Tabular values of opacity (Iglesias & Rogers 1993, 1996; Ferguson et al. 2005) and EoS (Rogers & Nayfonov 2002) are obtained by interpolation using the kap and eos modules of the MESA code (Paxton et al. 2011). Their dependence on the temperature is shown in Fig. 1 for two values of density ρ along with the analytical approximations. Figure 2 shows numerical differences between analytical and tabular opacities. The olive curve, superimposed on the diagram, represents the sequence of ρ and T obtained in our code for a disc around a $10 M_\odot$ central star. The cyan dot in the middle of it marks a boundary between thermally stable and unstable disc zones. It can be concluded that the Kramers law approximates better the tabular opacity in the hotter parts of the disc, while the ‘BL94’ works better for the colder parts, where $T_{\text{eff}} \sim (3 - 30) \times 10^3$ K.

2.3 Boundary conditions

We integrate system (1–4) starting from the surface of the disc, where $z = z_0$ and the optical depth $\tau = 2/3$. The boundary conditions there are as follows:

$$Q(z_0) = Q_0 \equiv Q_{\text{vis}}(z_0) = \frac{3}{8\pi} \frac{F\omega_K}{r^2}, \quad (7)$$

$$T(z_0) = T_{\text{eff}} \equiv (Q_0/\sigma_{\text{SB}})^{1/4}, \quad (8)$$

$$\Sigma(z_0) = 0. \quad (9)$$

Here $F = 2\pi r^2 W_{r\phi}$ is the viscous torque, and $W_{r\phi} \equiv \int_{-z_0}^{z_0} w_{r\phi} dz$ is the height-integrated viscous stress. In a stationary accretion disc the latter is derived from the angular momentum conservation and reads as follows:

$$F = \dot{M} h \left(1 - \sqrt{\frac{r_{\text{in}}}{r}} \right) + F_{\text{in}}, \quad (10)$$

where $h = \sqrt{GM}r$ is the specific angular momentum and F_{in} is the

viscous torque at the inner radius r_{in} (see e.g., Shakura et al. 2018). Below we assume $W_{r\phi}(r_{\text{in}}) = 0$. Notice that an arbitrary torque $F(r)$ can be set in the code.

To obtain the boundary condition for pressure, we write equation of hydrostatic equilibrium (1) in the photosphere:

$$\frac{dP}{d\tau} = \frac{\omega_K^2 z}{\kappa_R}, \quad (11)$$

where the optical depth τ is defined from:

$$d\tau = -\kappa_R \rho dz, \quad (12)$$

so that it increases from the surface to symmetry plane. Integrating equation (11) gives:

$$P_{\text{gas}}(z_0) + \frac{1}{2} P_{\text{rad}}(z_0) = \int_0^{2/3} \frac{\omega_K^2 z_0}{\kappa_R(P_{\text{gas}}, T(\tau))} d\tau, \quad (13)$$

where we use the grey Eddington approximation for the temperature: $T(\tau) = T_{\text{eff}}(1/2 + 3\tau/4)^{1/4}$. For a power-law opacity, the integral can be taken analytically (Ketsaris & Shakura 1998), provided that coordinate z hardly changes in the photosphere and equals to z_0 .

The half-thickness of the disc z_0 is a free parameter. Thus, we have to set one additional boundary condition at the symmetry plane of the disc ($z = 0$):

$$Q(0) = 0, \quad (14)$$

which follows from the symmetry of the problem.

2.4 Irradiation by central X-ray source

X-ray irradiation by the central accreting object (e.g., a neutron star) or by central parts of the accretion disc can be another source of heating, and even exceed the viscous heating at large radii.

The spectrum of the incident radiation plays a major role. Soft X-rays are absorbed relatively high in the disc atmosphere and heat up the chromosphere-like layer, while photons with energy > 3 keV can penetrate deep (Suleimanov et al. 1999). If they are absorbed in the layers below the photosphere (where the optical depth for the disc own emission $\tau \sim 2/3$), X-ray photons are thermalized and their energy is contributed to the flux outgoing from the photosphere.

The surface temperature rises in presence of irradiation, and the new boundary condition can be written in the form

$$T^4(z_0) = T_{\text{vis}}^4 + T_{\text{irr}}^4, \quad (15)$$

where irradiation temperature T_{irr} measures the additional heating by X-rays and will be defined differently in the two methods below. For irradiated discs we term (8) as ‘viscous temperature’

$$T_{\text{vis}} \equiv \left(\frac{Q_0}{\sigma_{\text{SB}}} \right)^{1/4}. \quad (16)$$

As we do not calculate an irradiated atmosphere model, we cannot calculate pressure from integral (13). Instead, following Tuchman et al. (1990) and Hameury et al. (1998), we assume that both the Rosseland opacity and z are constant in the photosphere and take the value of pressure evaluated at $\tau = 2/3$:

$$P_{\text{gas}}(z_0) + P_{\text{rad}}(z_0) = \frac{2}{3} \frac{\omega_K^2 z_0}{\kappa_R(P_{\text{gas}}(z_0), T(z_0))}. \quad (17)$$

We use two ways to include irradiation. In the first method, only boundary conditions are changed (an approach similar to that by Tuchman et al. 1990; Dubus et al. 1999), while in the second one equations are altered as well.

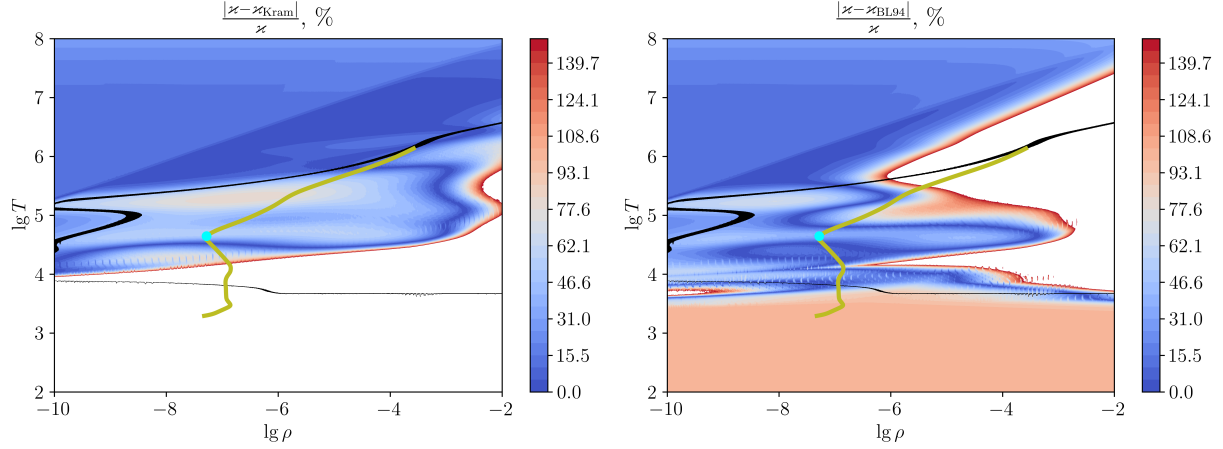


Figure 2. Shown are relative uncertainties between analytical approximations of opacity compared to tabular opacity values, obtained from MESA, as functions of density and temperature. Colour indicates the uncertainty in percents. In white regions the uncertainty is larger than 150%. The left panel shows the uncertainty relative to the Kramers opacity law, and the right one, to the approximations by Bell & Lin (1994) (see Sect. 2.2 for details). The black curve shows the range of ρ and T , where the electron scattering κ_T and absorption κ_{ff} opacity coefficients are equal. The olive curve shows the $\rho - T$ relation for disc around $10 M_{\odot}$ object, with turbulent parameter $\alpha = 0.1$ and accretion rate $\dot{M} = 10^{18} \text{ g s}^{-1}$, corresponding to Fig. 3 below; the dot on the curve indicates the parameters at the outer hot-zone radius.

2.4.1 (i) First method

In the first method, the boundary conditions on the temperature and pressure become (15) and (17). This roughly corresponds to all the heating caused by X-rays taking place at the photosphere level.

Irradiation temperature T_{irr} can be expressed in terms of irradiation parameter C_{irr} :

$$T_{\text{irr}}^4 = C_{\text{irr}} \frac{L_X}{4\pi\sigma_{\text{SB}}r^2}, \quad (18)$$

where $L_X = \eta \dot{M} c^2$ is the X-ray luminosity of the central source.

2.4.2 (ii) Second method

In the second method, X-ray radiation with arbitrary spectrum $F_X^{\nu}(\nu)$ penetrates into the disc and affects distributions of the energy flux $Q(z)$ and temperature $T(z)$. In the disc the additional source of heating appears, so that Eq. (2) changes to the following form:

$$\frac{dQ}{dz} = \frac{d(Q_{\text{vis}} + Q_{\text{irr}})}{dz} = \frac{3}{2} \omega_K \alpha P + \varepsilon, \quad (19)$$

where ε and Q_{irr} are the local heating rate of the disc through X-ray photons and the corresponding vertical energy flux. They are calculated from the analytical solution of radiation transfer equation for X-ray photons (see equations (17)–(21) in Mescheryakov et al. (2011) and Appendix A). Accordingly, the boundary condition on the flux is changed:

$$Q(z_0) = Q_0 + Q_{\text{irr}}(z_0). \quad (20)$$

The temperature and pressure boundary conditions are still (15) and (17), respectively.

While in the previous method the irradiation temperature or irradiation parameter can be an input parameter, now T_{irr} is calculated from calculated flux Q_{irr} (A5) at the photosphere level:

$$\sigma_{\text{SB}} T_{\text{irr}}^4 = Q_{\text{irr}}(z_0). \quad (21)$$

The system has two free parameters: z_0 and the surface density of the disc Σ_0 . Therefore, the code solves a two-parameter optimization problem and finds (z_0, Σ_0) . Contrary to the previous method, where

the surface density of the disc is obtained on solving the equations, now one has to set the additional boundary condition, complementary to (14):

$$\Sigma(z=0) = \Sigma_0. \quad (22)$$

We assume that X-ray radiation comes from the point-like central object, whose flux at distance r is:

$$F_X^{\nu}(r) = \frac{L_X}{4\pi r^2} S(\nu), \quad (23)$$

where $S(\nu)$ is the spectrum of incident X-ray flux (in units of 1/Hz or 1/keV and normalized to unity over a specified frequency range), and L_X is the X-ray luminosity of the central source. Both $S(\nu)$ and L_X can be set by user in the code (see Appendix B).

2.5 Calculation

We have developed Python 3 code that solves equations presented above. Code is open-source and available from GitHub² (see its short description in Appendix B). Several examples of calculated vertical structures can be found in Appendix C for different effective temperatures for cases with and without external irradiation.

We have checked the consistency of the code with results of some previous works. For analytic opacities the obtained vertical structure of un-irradiated disc agrees with results by Ketsaris & Shakura (1998) (see Tavleev et al. 2019, 2022). The irradiated disc structure agrees with results by Mescheryakov et al. (2011) and that by Dubus et al. (1999); Tuchman et al. (1990), for corresponding methods.

3 RADIAL STRUCTURE

Standard model of the disc accretion defines three radial zones (Shakura & Sunyaev 1973). In zone A, the radiation pressure is greater than the gas pressure, and opacity is determined by scattering. In zone B, the gas pressure is greater than the radiation

² <https://github.com/AndreyTavleev/DiscVerSt>

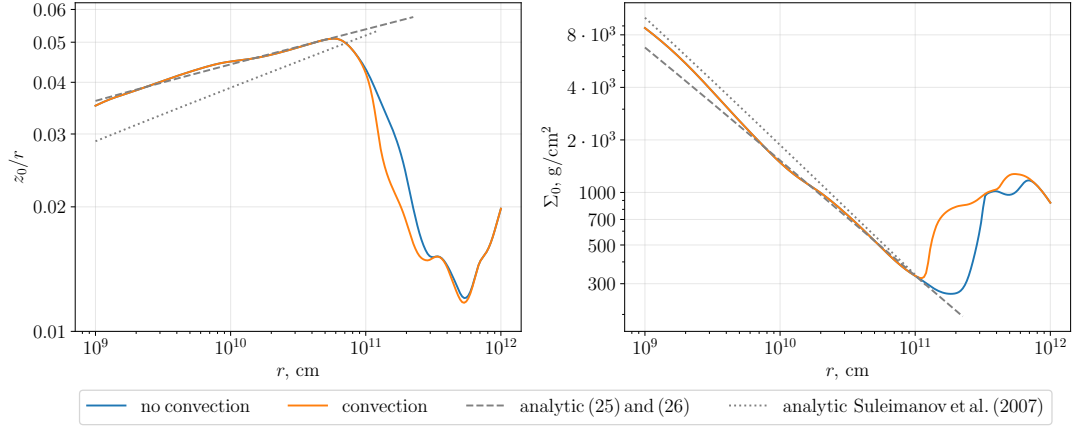


Figure 3. Radial structure of disc with $M = 10 M_{\odot}$, $\alpha = 0.1$, $\dot{M} = 10^{18} \text{ g s}^{-1}$, with and without convection together with theoretical approximations (25–26) and analytical approximations by Suleimanov et al. (2007). Shown are the semi-thickness of disc z_0/r and surface density Σ_0 . It can be seen that convection thins the unstable part of the disc.

pressure, but opacity is still determined by scattering. Finally, in zone C, opacity is determined by the absorption processes, and gas pressure is much greater than the radiation pressure.

Suleimanov et al. (2007) demonstrated that analytic radial dependencies of disc parameters in zones B and C could be written more accurately if solutions of vertical structure were taken into account. This approach relied on the method of vertical-structure calculation by Ketsaris & Shakura (1998) for analytical opacity coefficient and EoS, who introduced dimensionless Π -parameters. Here we write these parameters in a more general form:

$$\begin{aligned} \Pi_1 &\equiv \frac{\omega_K^2 z_0^2 \rho_c}{P_c}, & \Pi_2 &\equiv \frac{\Sigma_0}{2z_0 \rho_c}, \\ \Pi_3 &\equiv \frac{3 \alpha \omega_K P_c \Sigma_0}{4 \rho_c Q_0}, & \Pi_4 &\equiv \frac{3}{32} \left(\frac{T_{\text{eff}}}{T_c} \right)^4 \Sigma_0 z_c. \end{aligned} \quad (24)$$

Here P_c, T_c, ρ_c are the total pressure, temperature and bulk density in the symmetry plane. Values of Π -parameters can be found on solving the vertical structure for any opacity in a power-law form (Ketsaris & Shakura 1998; Malanchev et al. 2017).

Knowing Π -values, one can obtain from (24) analytical formulas for the radial distribution of $z_0/r, \Sigma_0, T_c, \rho_c$. It was done for Kramers and Thomson opacity in Suleimanov et al. (2007), see also Shakura et al. (2018).

As we have already mentioned in relation with Figures 1 and 2, near the outer boundary of the hot disc (see the cyan dot on the olive curve in Fig. 2), the opacity approximation $\kappa_R \sim \rho T^{-5/2}$ fits better the tabular opacity than the Kramers law ($\kappa_R \sim \rho T^{-7/2}$) does. Let us substitute the EoS of ideal gas in (24) along with the opacity approximation formula obtained by Bell & Lin (1994) for hot disc regions, where opacity is determined by free-free and bound-free transitions. We obtain:

$$z_0/r = 0.0207 m^{-13/36} \alpha^{-1/9} r_{10}^{1/12} \dot{M}_{17}^{1/6} f(r)^{1/6} \left(\frac{\mu}{0.6} \right)^{-13/36} \left(\frac{z_0}{z_0^*} \right)^{1/18} \Pi_z, \quad (25)$$

$$\Sigma_0 = 32 m^{2/9} \alpha^{-7/9} r_{10}^{-2/3} \dot{M}_{17}^{2/3} f(r)^{2/3} \left(\frac{\mu}{0.6} \right)^{13/18} \left(\frac{z_0}{z_0^*} \right)^{-1/9} \Pi_{\Sigma} [\text{g cm}^{-2}], \quad (26)$$

$$\rho_c = 7.8 \cdot 10^{-8} m^{7/12} \alpha^{-2/3} r_{10}^{-7/4} \dot{M}_{17}^{1/2} f(r)^{1/2} \left(\frac{\mu}{0.6} \right)^{13/12} \left(\frac{z_0}{z_0^*} \right)^{-1/6} \Pi_{\rho} [\text{g cm}^{-3}], \quad (27)$$

$$T_c = 4.1 \cdot 10^4 m^{5/18} \alpha^{-2/9} r_{10}^{-5/6} \dot{M}_{17}^{1/3} f(r)^{1/3} \left(\frac{\mu}{0.6} \right)^{5/18} \left(\frac{z_0}{z_0^*} \right)^{1/9} \Pi_T [\text{K}]. \quad (28)$$

Here:

$$\begin{aligned} m &\equiv \frac{M}{M_{\odot}}, & \dot{M}_{17} &\equiv \frac{\dot{M}}{10^{17} \text{ g s}^{-1}}, & r_{10} &\equiv \frac{r}{10^{10} \text{ cm}}, \\ z_0^* &\equiv 1.5 \cdot 10^{20} \text{ cm}^5 \text{ g}^{-2} \text{ K}^{5/2}, & f(r) &\equiv \frac{F}{\dot{M} h} = 1 - \sqrt{\frac{r_{\text{in}}}{r} + \frac{F_{\text{in}}}{\dot{M} h}}. \end{aligned} \quad (29)$$

Dimensionless parameters $\Pi_z, \Pi_{\Sigma}, \Pi_{\rho}, \Pi_T$ are almost constant in optically thick discs ($\tau \gtrsim 10^4$) and are as follows:

$$\begin{aligned} \Pi_z &= \Pi_1^{17/36} \Pi_2^{-1/18} \Pi_3^{1/9} \Pi_4^{-1/18} \approx 2.6, \\ \Pi_{\Sigma} &= \Pi_1^{1/18} \Pi_2^{1/9} \Pi_3^{7/9} \Pi_4^{1/9} \approx 1.049, \\ \Pi_{\rho} &= \Pi_1^{-5/12} \Pi_2^{-5/6} \Pi_3^{2/3} \Pi_4^{1/6} \approx 0.771, \\ \Pi_T &= \Pi_1^{-1/18} \Pi_2^{-1/9} \Pi_3^{2/9} \Pi_4^{-1/9} \approx 1.095. \end{aligned} \quad (30)$$

Figure 3 presents the radial structure of solar disc with and without convection together with analytical approximations (25–26) and Π_z, Π_{Σ} values (30), which are in good agreement with calculations in the stable region. One can see that Eq. (25) better describes the z_0/r -profile in the outer part of the hot disc than the analytical approximation by Suleimanov et al. (2007) does. Moreover, this approximation is better even for hotter part of the disc. This is due to the influence of radiation pressure ($P_{\text{rad}}/P_{\text{gas}} \sim 0.2$ at $r = 10^9$ cm), which causes the z_0/r -profile to “shift” higher compared to a calculation without taking into account radiation pressure.

Overall, our analysis shows that approximations (25)–(28) provide a reliable description (accuracy better than 15%) for z_0/r - and Σ_0 -profile in the outermost regions of the stationary hot disc if parameters fall in $M = 1 - 10 M_{\odot}$, $\alpha = 0.01 - 1.0$, $\dot{M} = 10^{-3} - 1.0 \dot{M}_{\text{edd}}$.

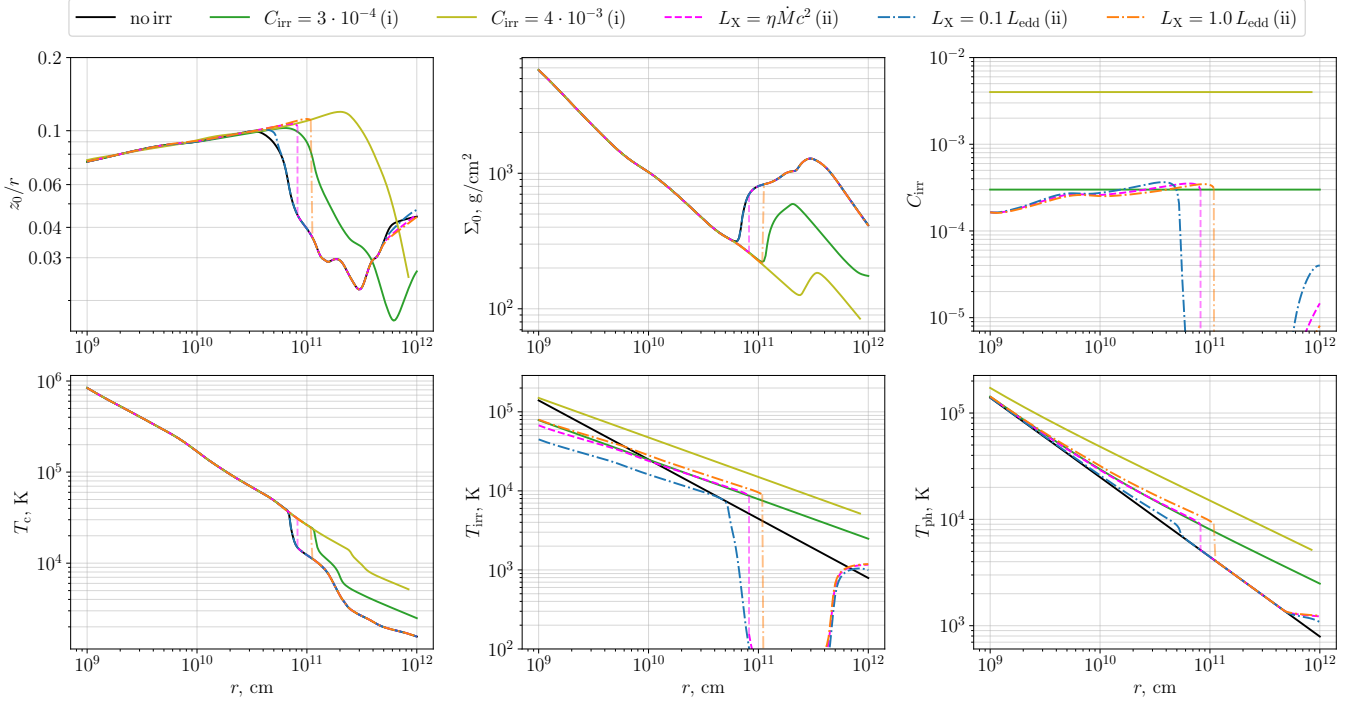


Figure 4. Radial profiles of the vertical height z_0/r , surface density Σ_0 , mid-plane temperature T_c , temperature at the photosphere T_{ph} , irradiation temperature T_{irr} and irradiation parameter C_{irr} for un-irradiated disc and irradiated disc with irradiation scheme (i) (see Sect. 2.4) for two C_{irr} , and with advanced scheme (ii) for different X-ray luminosities. Mass of central object $M = 1.4 M_{\odot}$, $\alpha = 0.1$, $\dot{M} = 10^{18} \text{ g s}^{-1} \approx 0.5 \dot{M}_{\text{edd}}$. The black line in lower figures shows the viscous temperature T_{vis} .

Specifically, these outermost regions are $(0.01 - 1) \times R_{\text{hot}}$ for z_0/r and $(0.1 - 1) \times R_{\text{hot}}$ for Σ_0 , where R_{hot} is the outer radius of the hot stable zone³. Furthermore, Eqs. (25)–(28) describe satisfactorily the quasi-stationary structure of outermost parts of an evolving fully-ionized disc, for example during an outburst, if function $f(r)$ from (29) is properly adjusted (see figure 1.19 and table 1.5 in Shakura et al. 2018).

It should be kept in mind that there are intervals in the radial dependencies in Fig. 3 that correspond to thermally-unstable solutions of the vertical structure. These intervals manifest themselves by sharp positive slope of the surface density radial profile. Thus, shown radial structure cannot hold longer than for a thermal time in unstable parts. Notice that account of the convection “shifts” the instability region to the smaller radii.

3.1 Irradiated disc

Figure 4 presents radial profiles of the relative semi-thickness z_0/r , surface density Σ_0 , mid-plane temperature T_c , temperature at the photosphere T_{ph} , irradiation temperature T_{irr} and irradiation parameter C_{irr} for un-irradiated and irradiated disc. Unless indicated otherwise, for the central X-ray luminosity $L_X = \eta \dot{M} c^2$ we assume accretion efficiency $\eta = 0.1$. Irradiation is taken into account by two methods (see Sect. 2.4: with scheme (i) for two values of C_{irr} (the dark and light green lines) and with advanced scheme (ii) for different X-ray luminosities (the blue, orange, and magenta lines).

In scheme (ii), for spectrum of incident X-rays in expression (23)

we take:

$$S(\nu) \propto \left(\frac{E}{kT_{\text{sp}}} \right)^{-0.4} \exp \left(- \frac{E}{kT_{\text{sp}}} \right) \quad (31)$$

in the range 1 – 10 keV, with $T_{\text{sp}} = 8 \text{ keV}$ (Mescheryakov et al. 2011). Note that spectrum $S(\nu)$ is the parameter of the code and can be set manually (see Appendix B). The incident angle of external irradiation is assumed to be

$$\cos \theta_0 \approx \frac{dz_0}{dr} - \frac{z_0}{r} = \frac{z_0}{r} \left(\frac{d \ln z_0}{d \ln r} - 1 \right) = \frac{1}{12} \frac{z_0}{r}, \quad (32)$$

following the analytical approximation (25) for z_0/r in the case of a steady disc, when $f(r) \approx 1$.

It is known that $f(r)$ differs from 1 for quasi-stationary hot zones of discs during outbursts (Shakura et al. 2018, figure 1.19) and its analytical form may be used in (32). On the other hand, the height where the X-rays are effectively intercepted may differ from z_0 remarkably. This can be due to scattering above the disc (Suleimanov et al. 2007; Mescheryakov et al. 2011). Possible changes to (32) are allowed in the code, see Appendix B.

Interestingly, a physically reasonable result is reproduced even with the incident angle (32) for a shadowed zone beyond the hot ionized one. This happens because the calculated value of C_{irr} drops there, see also section 3.1.2.

3.1.1 Comparing results of methods for irradiated disc

In confirmation with results of previous works (e.g., Dubus et al. 1999), strong irradiation keeps the disc in the hot state at farther distances, comparing to the case without irradiation. We find that

³ R_{hot} can be found using (35) from \dot{M} , α , and M .

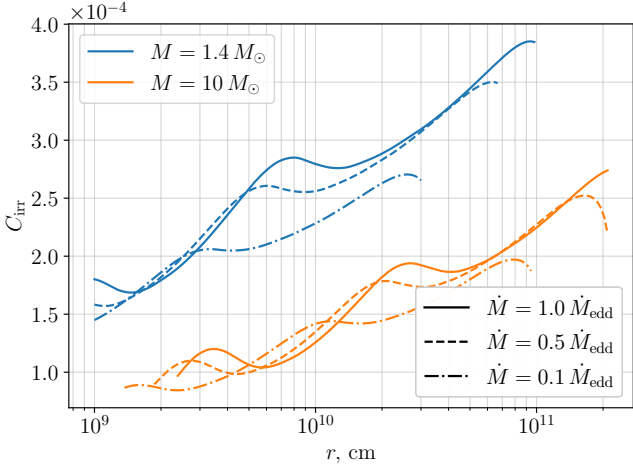


Figure 5. Radial profile of irradiation parameter C_{irr} for two masses ($M = 1.4, 10 M_{\odot}$) and three accretion rates ($\dot{M} = 0.1, 0.5, 1 \dot{M}_{\text{edd}}$), $\alpha = 0.1$.

irradiation method slightly affects the hot disc size. For comparable values of Q_{irr} , cf. the dark green and magenta lines in Fig. 4, the hot disc has very similar radial extension, which is seen in the panel for Σ as a location where the surface density starts to rise going outwards. Additionally, there is difference in the relative thickness profiles: the disk calculated in scheme (i) becomes shadowed at smaller radius, whereas scheme (ii) yields shielding right at the hot zone radius.

Furthermore, stabilization of the disc’s vertical structure by irradiation with $T_{\text{irr}} \gtrsim 10^4$ K, previously found by Tuchman et al. (1990); Dubus et al. (1999), occurs in our calculations by either irradiation method. The temperature of the stability loss, which is actually $\lesssim 9000$ K, is investigated by us in detail in section 5.

3.1.2 Value of C_{irr}

The irradiation parameter C_{irr} and irradiation temperature T_{irr} for advanced scheme (ii), also shown in Fig. 4, can be calculated from the flux Q_{irr} (see (21) and (A8)). One can see that both C_{irr} and T_{irr} drop dramatically in the region where $T_{\text{irr}} < 9000$ K. On comparing the curves for C_{irr} with disc profiles, we infer that the drop of C_{irr} is not due to a purely geometrical effect, since the cosine between incident rays and normal to the disc surface, which is set proportional to z_0/r according to (32), decreases by only a few times. We deduce that the drop happens due to strong absorption of X-ray photons above the disc photosphere, so that the external irradiation hardly affects the disc vertical structure. This increased absorption is driven by a very high column density in the photosphere of the outer part of a disc (see the dashed line in Fig. 6), which, in its turn, results from setting $\dot{M} = \text{const}$ at all radii.

According to expression (A2) and (A9), C_{irr} value depends on the X-ray spectrum, angle of incident rays and optical depth to X-rays above the level where the optical flux $\sigma_{\text{SB}} T_{\text{vis}}^4$ is formed (it is $\tau = 2/3$ in our scheme). As we show in Appendix A for single-frequency X-ray photons, if the column density of the photosphere layer above the disc surface $\Sigma_{\text{ph}} = 0$ and the total optical thickness of the disc $\tau_0 \gg 1$, one obtains analytically that $C_{\text{irr}} = (1 - A) \cos \theta_0$, where A is the frequency-dependent albedo (see Eq. (A10) and equation A39 in Mescheryakov et al. (2011)). This is in agreement with the previously proposed definition of C_{irr} , according to which, for a point-like source, the irradiation parameter can be written as (e.g., Suleimanov

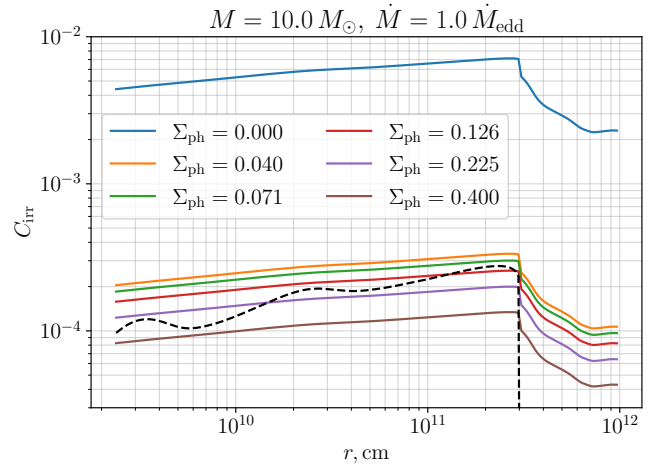


Figure 6. Radial profile of C_{irr} , when the column density of the photosphere layer above the disc surface $\Sigma_{\text{ph}} = \text{const}$ (coloured solid lines) in contrast with realistic C_{irr} profile (the black dashed line). System parameters are $M = 10 M_{\odot}$, $\dot{M} = 1 \dot{M}_{\text{edd}}$, $\alpha = 0.1$. The legends give the photosphere column density in g cm^{-2} . Drop of C_{irr} on the left occurs in the zone of the disc where the vertical structure is unstable.

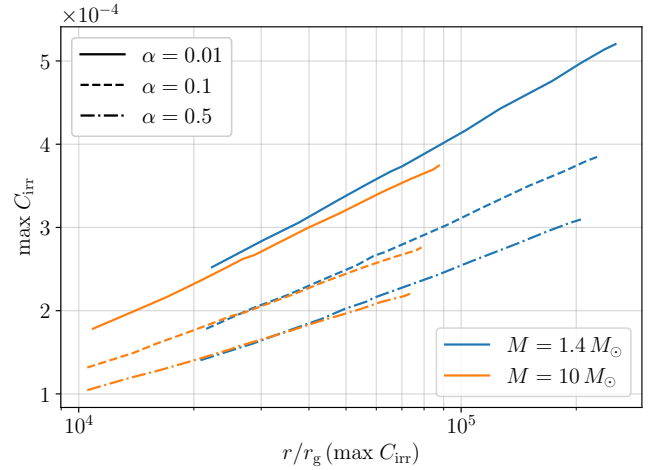


Figure 7. Maximum C_{irr} for accretion rates $(10^{-2} - 1) \dot{M}_{\text{edd}}$, as function of the radius (in Schwarzschild radius) for two central source masses (different colours) and three α -parameters (different styles). Irradiation is taken into account by method (ii) and $L_X = \eta \dot{M} c^2$.

et al. 2007)

$$C_{\text{irr}} = (1 - A) \frac{z_0}{r} \left(\frac{d \ln z_0}{d \ln r} - 1 \right), \quad (33)$$

where $1 - A$ is the fraction of incoming X-ray flux that is subject to thermalization.

Fig. 5 shows radial dependencies of the irradiation parameter for different masses and accretion rates for the fixed spectrum (31). We stress that C_{irr} depends on the the upper boundary condition that defines Σ_{ph} and determines the pressure condition (17). The dependence $\Sigma_{\text{ph}}(r)$ is what drives the radial ‘wiggles’ of C_{irr} in Fig. 5: fixing photosphere column density to a constant value provides much more smooth C_{irr} behaviour, see Fig. 6. An additional analysis

showed that the dependence of the solid lines on radius in Fig. 6 came solely from the disc opening angle $z_0(r)/r$.

One could expect that $C_{\text{irr}} \propto z_0/r$. If albedo A in (33) is constant then a new parameter \tilde{C}_{irr} can be suggested via

$$C_{\text{irr}} = \tilde{C}_{\text{irr}} \frac{z_0}{r}, \quad (34)$$

see, e.g., [Lipunova et al. \(2022\)](#). Fig. A1 in the Appendix shows the radial profile of \tilde{C}_{irr} . Indeed the variability of \tilde{C}_{irr} with radius is less than that of C_{irr} . However, \tilde{C}_{irr} appears to depend on the accretion rate, which, possibly, is due to a nontrivial dependence of Σ_{ph} and A on \dot{M} . Auxiliary calculations have shown that, for varying value of the turbulent parameter α , from 0.01 to 0.5, the value of \tilde{C}_{irr} changes by only about $\pm 5\%$. However, the particular result is model-dependent and relies on the approximate boundary condition used in scheme (ii).

4 S-CURVES

[Meyer & Meyer-Hofmeister \(1981\)](#) have established that dependencies $F - \Sigma_0$ (S-curves) show the disc instability: the branch of the S-curve with a negative slope represents solutions to the vertical structure equations which are viscously unstable, i.e. oscillations have to develop during characteristic time of order of the viscous time. [Smak \(1982b, 1984\)](#) has showed that the viscously-unstable branch of the S-curve is also thermally unstable. Note that since the quasi-stationary discs has an unambiguous relation between F , \dot{M} and T_{eff} (see Eqs. (7), (8), (10)), the S-curve can be drawn also in coordinates $\dot{M} - \Sigma_0$ and $T_{\text{eff}} - \Sigma_0$.

An example of an S-curve calculated by our code is shown in Fig. 8, the top left panel. Arrows shows schematically the direction of ring evolution when an outburst happens ([Frank et al. 2002](#); [Done et al. 2007](#); [Kato et al. 2008](#)): if in initially cold disc the surface density and temperature gradually rise ('a' \rightarrow 'b'), they eventually reach the critical point 'b', where $T_{\text{eff}} \sim 7000$ K and $T_c \sim 13000$ K. The further temperature increase leads to a runaway heating: the thermal instability develops and brings the ring to the upper branch. There, a rapid viscous evolution occurs ('e' \rightarrow 'd'). The surface density decreases and the ring reaches the critical point 'd' beyond which no stable 'hot' solution is possible, and the ring transits to neutral 'cold state'. Note a very different opacity dependence on the temperature in the upper and central layers of the disc for the unstable state (see the right panel of Fig. 8, the dashed pieces; also [Faulkner et al. \(1983\)](#)). This illustrates that irradiation of a hot decaying disc may inhibit an onset of instability by keeping the upper disc layer hot.

We have computed several thousand S-curves for α from $3 \cdot 10^{-4}$ to 0.7, M from $1 M_{\odot}$ to $20 M_{\odot}$ and r from $7 \cdot 10^7$ cm to $5 \cdot 10^{11}$ cm and obtained the turning points Σ^+ and Σ^- , T_{eff}^+ and T_{eff}^- , \dot{M}^+ and \dot{M}^- , denoted below as 'TP', which define the upper and lower S-curve turns, respectively. The chemical composition is assumed to be solar, and convective energy transport is taken into account. We fit the resulting TPs as:

$$f(M, \alpha, r) = A \left(\frac{M}{M_{\odot}} \right)^{\beta} \alpha^{\gamma} \left(\frac{r}{10^{10} \text{ cm}} \right)^{\delta}, \quad (35)$$

where the parameters A, β, γ, δ and average relative uncertainty of TPs can be found in [Table 2](#). The average relative uncertainty Δ is defined as

$$\Delta = \left\langle \frac{|f(M, \alpha, r) - \text{TP}|}{\text{TP}} \right\rangle_{M, \alpha, r}. \quad (36)$$

We find that these approximations of S-curves are generally close

Table 1. Comparison of S-curve turning points (TP) with previous results. The minimum, maximum, and mean relative differences are shown. Negative difference value means that our TP approximation (35) is less than the previous one.

TP		(min; max)	mean
Σ^+	L08 ^a	(15.2; 33.8)%	24.5%
	CW84 ^b	(18.2; 54.9)%	14.7%
	H98 ^c	(1.9; 13.3)%	7.7%
Σ^-	L08	(-5.5; 69.4)%	29.9%
	CW84	(-48.4; 25.2)%	8.1%
	H98	(-17.1; 7.8)%	4.9%
T_{eff}^+	L08	(2.9; 13.9)%	8.3%
T_{eff}^-	L08	(6.4; 21.4)%	13.1%

^a [Lasota et al. \(2008\)](#)

^b [Cannizzo & Wheeler \(1984\)](#)

^c [Hameury et al. \(1998\)](#)

to the previous ones ([Cannizzo & Wheeler 1984](#); [Hameury et al. 1998](#); [Lasota et al. 2008](#); [Hameury 2020](#), see [Table 1](#)). Taking into account that [Liu & Meyer-Hofmeister \(1997\)](#) have shown that the improved tabular opacities do not affect much the S-curves, we tend to conclude that uncertainties in Σ_0 are related to the slightly different boundary condition for pressure at the disc surface. The boundary condition (17) is used in previous works, while we use (13) instead. Other possible source of uncertainty is the EoS tables. [Lasota et al. \(2008\)](#) used tables from ([Fontaine et al. 1977](#)), while we use OPAL EoS tables ([Rogers & Nayfonov 2002](#)).

4.1 Irradiation and S-curves

[Figure 9](#) illustrates the influence of external irradiation on the disc stability. Considering the S-curves, calculated through scheme (i) for different irradiation temperatures T_{irr} , we infer that the unstable branch shrinks with the increase of T_{irr} . For $T_{\text{irr}} \gtrsim 10000$ K the unstable branch disappears, so the strong irradiation stabilizes the disc, which is in agreement with the previous works (e.g., [Tuchman et al. 1990](#); [Dubus et al. 1999](#)).

In scheme (ii), the irradiation temperature T_{irr} varies along the upper branch of the S-curve for compliant luminosity (the magenta line). It hardly varies for the orange and blue line (with fixed L_X), which is in accordance with C_{irr} being hardly dependent on \dot{M} , see [Fig. 5](#). On the lower and middle branch, T_{irr} in scheme (ii) is very low because significant part of X-rays are absorbed above the disc photosphere, see section 3.1.2.

The disc calculated with advanced irradiation scheme (ii) and self-consistent X-ray luminosity (magenta line) loses its stability when $T_{\text{irr}} = T_{\text{irr, crit}} \approx 7500$ K, $T_{\text{eff}} \approx 6600$ K and $\dot{M} \approx 0.06 \dot{M}_{\text{edd}}$. This critical value $T_{\text{irr, crit}}$ is lower than the one obtained in method (i) and by [Tuchman et al. \(1990\)](#); [Dubus et al. \(1999\)](#). Furthermore, it depends on disc parameters, as we show in section 5, see also [Fig. 11](#). Note that in case with $L_X = 0.1 L_{\text{edd}}$ the negative slope branch is numerically unstable and cannot be calculated reliably, which leads to S-curve discontinuity.

4.2 Influence of chemical composition, α parameter and convection on the shape of S-curves in X-ray transients

[Figure 10](#) shows S-curves for different chemical composition and α parameter. Curves with and without convection are also shown. The

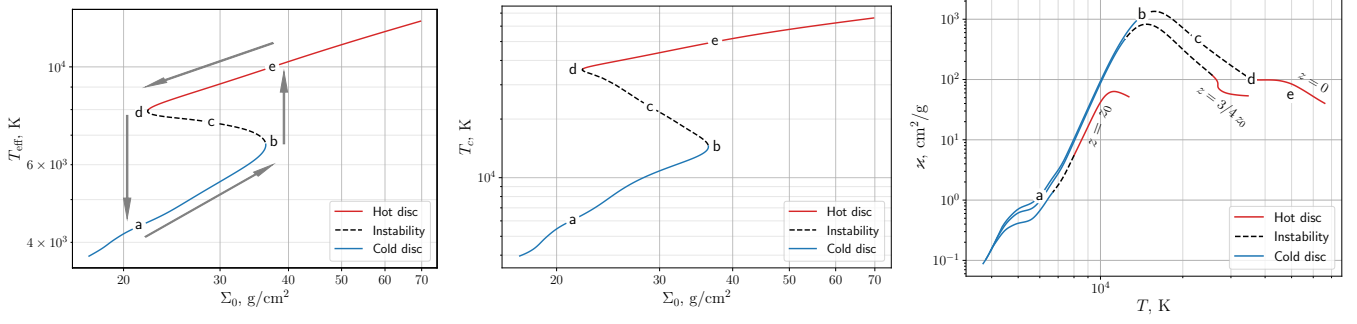


Figure 8. S-curve for $M = 10 M_{\odot}$, $\alpha = 0.1$, $r = 10^{10}$ cm and tabular opacities with solar chemical composition. The limit cycle is schematically shown by arrows. Also shown is the corresponding dependence of the symmetry plane temperature T_c and the opacity coefficient as a function of temperature at the symmetry plane of the disc ($z = 0$), at the disc surface ($z = z_0$) and in between ($z = 3/4 z_0$). The cold disc region, the region in which the instability takes place, and the region of the hot disc are marked with different style.

	A	β	γ	δ	Δ
Σ^+	$8.44 \pm 0.01 \text{ g cm}^{-2}$	-0.3674 ± 0.0006	-0.7821 ± 0.0002	1.1105 ± 0.0002	3.3%
Σ^-	$11.87 \pm 0.03 \text{ g cm}^{-2}$	-0.3723 ± 0.0009	-0.8405 ± 0.0003	1.1223 ± 0.0003	5.4%
\dot{M}^+	$(1.027 \pm 0.003) \cdot 10^{16} \text{ g s}^{-1}$	-0.843 ± 0.001	-0.0193 ± 0.0004	2.6258 ± 0.0003	5.4%
\dot{M}^-	$(5.065 \pm 0.016) \cdot 10^{15} \text{ g s}^{-1}$	-0.833 ± 0.001	0.0066 ± 0.0004	2.6038 ± 0.0004	6.5%
T_{eff}^+	$7341 \pm 2 \text{ K}$	0.0290 ± 0.0001	-0.00484 ± 0.00004	-0.08426 ± 0.00004	0.7%
T_{eff}^-	$6152 \pm 4 \text{ K}$	0.0315 ± 0.0002	0.00165 ± 0.00008	-0.08977 ± 0.00007	1.3%

Table 2. Values of the parameters (with standard deviations), which fit the S-curve turning points, where the '+' and '-' superscripts denote the upper and lower turning points, respectively. The right column contains the average relative uncertainty Δ of the turning points.

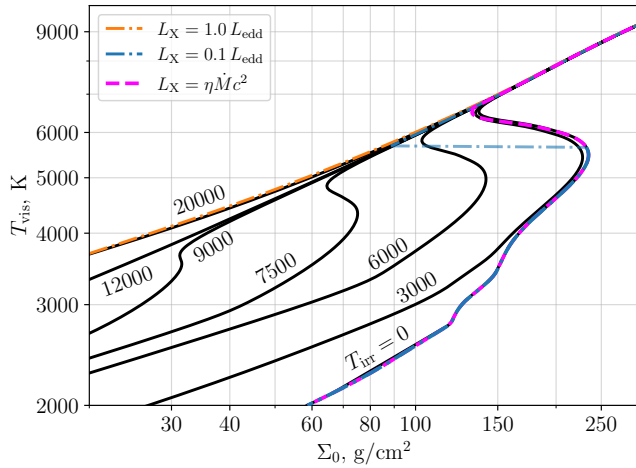


Figure 9. S-curves for irradiated discs. Black curves are calculated through scheme (i) with different irradiation temperatures T_{irr} . Coloured lines are the curves with irradiation, calculated with advanced scheme (ii). The magenta line corresponds to self-consistent luminosity of irradiation source $L_X = \eta \dot{M} c^2$, while the blue and orange lines corresponds to luminosities $L_X = 0.1, 1.0 L_{\text{edd}}$. All curves are calculated for $M = 1.4 M_{\odot}$, $r = 3 \cdot 10^{10}$ cm, $\alpha = 0.1$ and solar chemical composition.

dots mark the regions where convection in the disc dominates (i.e. the condition for the existence of convection $\nabla_{\text{rad}} > \nabla_{\text{ad}}$ is fulfilled in more than 50% over Σ). It is seen that the disc is convective in the unstable region.

According to [Faulkner et al. \(1983\)](#), convection does not affect the

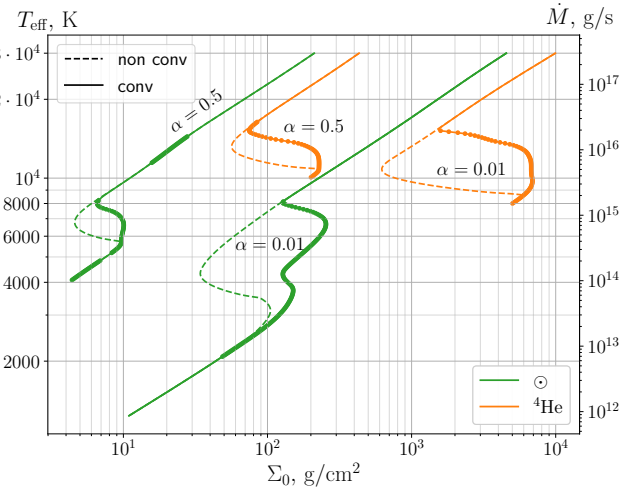


Figure 10. S-curves, for different chemical composition, α , with and without convection. All curves are calculated for $M = 10 M_{\odot}$ and $r = 10^{10}$ cm. Bold point regions are the zones where the disc is convective (i.e. the condition for the existence of convection $\nabla_{\text{rad}} > \nabla_{\text{ad}}$ is fulfilled over an Σ -range of more than 50%). Note that only the optically thick branches of the curves are shown. For this reason, the curves for the helium disc do not show the area corresponding to the cold disc, since it is optically thin.

very existence of instability. Indeed, we also obtain that, when the convection is ignored in the calculation, there is one unstable branch, regardless of the chemical composition or α .

When convection is taken into account, the instability starts at higher accretion rates. For large α , regions with convection are

“pulled” towards large Σ , and an almost vertical interval at lower unstable branch is formed. For small α , the convective branch splits into two unstable branches. In this case, the upper unstable branch is due to a peak in opacity related to the partial ionization of hydrogen. The lower branch is associated with convection (Cannizzo 1992) and with the formation of molecular hydrogen (Smak 1982b), see small peak in opacity (Fig. 1) at $T \approx 4000 - 5000$ K. This ‘wiggle’ is not usually associated with the outburst mechanism since the α -value is believed to change only when the ionization degree is changing. At large α , the lower unstable branch does not appear, since the temperature does not reach such low values, at which the formation of molecules begins.

On the S-curve for helium disc, the instability is related with partial ionization of helium, so the corresponding temperatures are larger than for solar and hydrogen disc. At both large and small α , the second unstable branch does not appear, only the main unstable branch is deformed.

These results for solar discs are consistent with the results in Cannizzo et al. (1982), where S-curves were investigated taking into account convection, which led to the appearance of additional kinks on the curve.

5 DISCUSSION

Values of C_{irr} , calculated by our code, are comparable or smaller than those suggested in previous works. For specific X-ray spectrum, calculated irradiation parameter C_{irr} is in the range $(1 - 5) \times 10^{-4}$ (Fig. 7). Esin et al. (2000) obtain $C_{\text{irr}} \sim 0.004$ by analyzing the light curves of soft X-ray transient A0620-00 (1975), and $C_{\text{irr}} \approx 0.0014$ for GRS 1124-68 (1991). Those values are consistent with estimate $C_{\text{irr}} \sim (2 - 4) \times 10^{-3}$ found by (de Jong et al. 1996) for some Low-Mass X-ray Binaries. On the other hand, Suleimanov et al. (2008b) for the same two transients obtain $C_{\text{irr}} \sim 7 \times 10^{-4}$ and $C_{\text{irr}} \sim 3 \times 10^{-4}$, respectively. Lipunova & Malanchev (2017) estimate that $C_{\text{irr}} \sim (3 - 6) \times 10^{-4}$ using optical data of 4U 1543-47 (outburst of 2002). Assuming the DIM model, Coriat et al. (2012) have analysed transient and persistent X-ray sources with neutron stars and black holes and concluded that irradiation parameter lies in the interval $10^{-3} - 10^{-2}$. This is an order of magnitude higher than the values obtained by us.

There is a physical reason of why our irradiation scheme provides the lower limit on C_{irr} . The present scheme involves neither additional heating of the disc by soft-X-rays-heated upper layers of the photosphere (above $\tau = 2/3$) nor the increased X-ray flux due to scattering in even higher and hotter corona (see Suleimanov et al. 2007; Mescheryakov et al. 2011). For supersoft X-ray sources, Suleimanov et al. (2003) suggest that relatively dense blobs immersed in a corona enable multiple X-ray or far-UV scattering which leads to observed large optical and UV fluxes. The same mechanism might increase the irradiation parameter C_{irr} .

The self-irradiation plays a crucial role in an outburst dynamics, since the hot disc size affects directly the duration of an outburst (see e.g., King & Ritter 1998). It was shown before that there is a minimum irradiation temperature that ensures the disc stability (Tuchman et al. 1990; Dubus et al. 1999), estimated as $(9 - 10) \times 10^3$ K. While the actual C_{irr} can be higher comparing to the values we find, the critical disc irradiation temperature, which switches on/off ionization instability, can be reliably obtained, since it depends not on C_{irr} but on how much the irradiation flux exceeds the internal viscous one.

In Fig. 11 we show dependence of the critical irradiation temperature on the ratio of the irradiation to viscous heat. For this we have

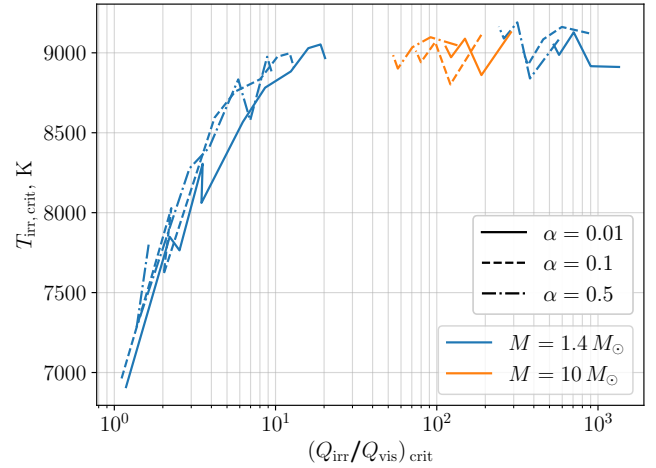


Figure 11. Critical value of irradiation temperature $T_{\text{irr,crit}}$, above which the disc is stable, as function of the ratio between irradiation and viscous heat $Q_{\text{irr}}/Q_{\text{vis}}$ for two central source masses (different colours) and three α -parameters (different styles). Irradiation is taken into account by method (ii). Note that weak irradiation does not affect the disc around $10 M_{\odot}$, so there is no $T_{\text{irr,crit}}$ in this case.

calculated numerous models of irradiated disc with scheme (ii), with arbitrary values of the central flux (to cover the scenarios of enhanced values of C_{irr}).

For strongly illuminated discs, when $Q_{\text{irr}} > Q_{\text{vis}}$, irradiation controls the disc size. This occurs for big discs and sufficiently high C_{irr} , suitably illustrated by a formula from Suleimanov et al. (2007):

$$\frac{Q_{\text{irr}}}{Q_{\text{vis}}} = \frac{4}{3} \eta C_{\text{irr}} \frac{r}{r_g}. \quad (37)$$

Thus, at radii $r > 3/4 r_g / (\eta C_{\text{irr}})$ the stability condition is $T_{\text{irr}} > T_{\text{irr,crit}}$, see Fig. 11.

In the opposite case, if $Q_{\text{irr}} < Q_{\text{vis}}$, irradiation does not affect the disc structure and the disc stability: unstable state is triggered at the radius where the effective temperature lowers to T_{eff}^+ . This can happen in the case of relatively small discs or small C_{irr} .

5.1 Code limitations

The code has been tested for discs with $T_{\text{eff}} \sim (10^3 - 10^6)$ K around stellar-mass central sources. The code can also be used to calculate discs around supermassive black holes (SMBH), where a specific zone B^* appears, a mixture of A and C disc zones (Burderi et al. 1998, see also Sect. 3). Note that the disc self-gravity becomes important when

$$\frac{2\pi G \Sigma}{\omega_K^2 z_0} > 1. \quad (38)$$

Inequality (38) is not checked automatically in the code, so this needs to be checked separately.

When $P_{\text{rad}} \gtrsim P_{\text{gas}}$, a thermal-viscous instability (Lightman & Eardley 1974; Shakura & Sunyaev 1976) appears and, accordingly, the solution of system (1)–(4) becomes problematic. Additionally, at high accretion rates, the local energy balance breaks: the energy is effectively transported in radial direction with the advected portion being of order of $(z_0/r)^2$. Our code does not calculate such discs.

While we present radial profiles and S-curves with a constant α -parameter, it should be noted that α is expected to vary. For example,

Smak (1984) showed that α should be lower by a factor of several in the ‘cold’ zone where $T_{\text{eff}} < 5000$ K. The change in the turbulent parameter is dictated by the need to produce outbursts of observed amplitude (see e.g., Hameury et al. 2009). Observations show that $\alpha \sim 0.1 - 1$ for the hot disc and $\alpha \sim 0.01$ for the cold disc (see, e.g., Cannizzo et al. 1988; Suleimanov et al. 2008a; Kotko & Lasota 2012; Martin et al. 2019; Tetarenko et al. 2018).

MRI simulations provide intriguing details (see, e.g. Hirose et al. 2014; Scepi et al. 2018; Jiang & Blaes 2020): α is higher near the upper turn of S-curve. The mechanism for such an increase is likely convection associated with the hydrogen ionization transition. In regions with high temperature, where convection does not occur, α remains low. However, there is no simple relationship between α and the strength of convection (Scepi et al. 2018).

Equation (2) of the viscous heating implies the local version of the α -prescription for viscosity, where the local tensor of viscous stress $w_{r\phi}$ is proportional to the total pressure. However, this is not always a good approximation, particularly in the layers where $\tau < 1$ (Shaviv & Wehrse 1986). An alternative form of α -viscosity is the global form, where the vertically integrated viscous stress $W_{r\phi}$ is proportional to the vertically averaged total pressure. This form is used, e.g., in calculations of disc spectra (Hubeny & Long 2021).

Another important point is the pressure boundary condition, which is very approximate due to a simple atmospheric model used. Its proper determination requires the accurate calculation of the disc spectrum (see, e.g., Hubeny & Long 2021). We treat the atmosphere in the Eddington approximation and use the boundary condition for pressure (13) or (17). These two approaches give boundary pressure 70% apart from each other in the unstable convective region, leading to differences in values at the turning points (see Sect. 4).

6 SUMMARY

Calculation of the vertical structure of accretion discs is necessary to understand stability properties of accretion discs and to reconstruct the light curves of X-ray transients. Large range of physical conditions over a disc or various chemical composition in different objects require a numerical approach of calculating disc parameters, which is fast and flexible at the same time. Our first open numerical code for the model of the vertical structure with different types of equation of state and opacity laws, including tabular values, takes into account both radiative and convective energy transport and external X-ray irradiation.

Using the results of numerical models, we obtain analytical formulas for radial dependencies of disc parameters using Bell & Lin (1994) power-law approximation of opacity coefficient in the high-temperature plasma. These formulas can be applied in the outermost parts of a hot ionized accretion disc around a stellar-mass compact object.

We analyse stability criteria for our disc model. For this, analytical approximations for the S-curve turning points are obtained. Comparing to previous results, variations in Σ_0 turning points are explained by slightly different boundary condition for pressure at the disc surface and different EoS tables.

For a case with external X-ray irradiation, stabilization of the disc’s vertical structure at $T_{\text{irr}} > 10^4$ K, previously found by Tuchman et al. (1990); Dubus et al. (1999), occurs in our models as well. Using the advanced scheme of calculation of irradiation disc vertical structure, we refine the critical value of T_{irr} and find that it changes in range 6900 – 9000 K. We propose its unique dependence on the ratio between irradiation and viscous heat (Fig.11). In addition, we

calculate values of self-irradiation parameter C_{irr} in our model. They represent lower estimates of the actual C_{irr} in X-ray transients, since additional heating and/or scattering from the hot layers above the disc photosphere should enhance the heating effect.

ACKNOWLEDGEMENTS

The authors are grateful to Valery Suleimanov for discussion and the referee for helpful suggestions. The work was supported by the RSF grant 21-12-00141.

DATA AVAILABILITY

Code for calculating the vertical structure is open-source and available from GitHub⁴.

The pre-calculated S-curve turning points (Σ^+ and Σ^- , T_{eff}^+ and T_{eff}^- , \dot{M}^+ and \dot{M}^-) are available⁵ for 20 linearly scaled values of M from $1 M_{\odot}$ to $20 M_{\odot}$, 20 logarithmically scaled values of α from $3 \cdot 10^{-4}$ to 0.7, 20 logarithmically scaled values of r from $7 \cdot 10^7$ cm to $5 \cdot 10^{11}$ cm.

REFERENCES

- Alexander D. R., 1975, *ApJS*, 29, 363
 Astropy Collaboration et al., 2013, *A&A*, 558, A33
 Astropy Collaboration et al., 2018, *AJ*, 156, 123
 Badnell N. R., Bautista M. A., Butler K., Delahaye F., Mendoza C., Palmeri P., Zeppen C. J., Seaton M. J., 2005, *MNRAS*, 360, 458
 Bagińska P., Róžańska A., Czerny B., Janiuk A., 2021, *ApJ*, 912, 110
 Bell K. R., Lin D. N. C., 1994, *ApJ*, 427, 987
 Burderi L., King A. R., Szuszkiewicz E., 1998, *ApJ*, 509, 85
 Cannizzo J. K., 1992, *ApJ*, 385, 94
 Cannizzo J. K., Wheeler J. C., 1984, *ApJS*, 55, 367
 Cannizzo J. K., Ghosh P., Wheeler J. C., 1982, *ApJ*, 260, L83
 Cannizzo J. K., Shafter A. W., Wheeler J. C., 1988, *ApJ*, 333, 227
 Coriat M., Fender R. P., Dubus G., 2012, *MNRAS*, 424, 1991
 Cox A. N., Stewart J. N., 1969, *Nauchnye Informatsii*, 15, 1
 Cox A. N., Tabor J. E., 1976, *ApJS*, 31, 271
 Done C., Gierliński M., Kubota A., 2007, *A&ARv*, 15, 1
 Dubus G., Lasota J.-P., Hameury J.-M., Charles P., 1999, *MNRAS*, 303, 139
 Dubus G., Hameury J. M., Lasota J. P., 2001, *A&A*, 373, 251
 Esin A. A., Kuulkers E., McClintock J. E., Narayan R., 2000, *ApJ*, 532, 1069
 Faulkner J., Lin D. N. C., Papaloizou J., 1983, *MNRAS*, 205, 359
 Ferguson J. W., Alexander D. R., Allard F., et al., 2005, *ApJ*, 623, 585
 Fontaine G., Graboske H. C. J., van Horn H. M., 1977, *ApJS*, 35, 293
 Frank J., King A., Raine D. J., 2002, *Accretion Power in Astrophysics: Third Edition*
 Hameury J. M., 2020, *Advances in Space Research*, 66, 1004
 Hameury J.-M., Menou K., Dubus G., et al., 1998, *MNRAS*, 298, 1048
 Hameury J. M., Viallet M., Lasota J. P., 2009, *A&A*, 496, 413
 Hirose S., Blaes O., Krolik J. H., Coleman M. S. B., Sano T., 2014, *ApJ*, 787, 1
 Hōshi R., 1979, *Progress of Theoretical Physics*, 61, 1307
 Hubeny I., Long K. S., 2021, *MNRAS*, 503, 5534
 Hunter J. D., 2007, *Computing in Science & Engineering*, 9, 90
 Iglesias C. A., Rogers F. J., 1993, *ApJ*, 412, 752
 Iglesias C. A., Rogers F. J., 1996, *ApJ*, 464, 943
 Jiang Y.-F., Blaes O., 2020, *ApJ*, 900, 25

⁴ <https://github.com/AndreyTavleev/DiscVerSt>

⁵ <https://doi.org/10.5281/zenodo.7361425>

- Jones E., Oliphant T., Peterson P., et al., 2001–2019, SciPy: Open source scientific tools for Python, <http://www.scipy.org/>
- Kato S., Fukue J., Mineshige S., 2008, *Black-Hole Accretion Disks — Towards a New Paradigm* —
- Ketsaris N. A., Shakura N. I., 1998, *Astronomical and Astrophysical Transactions*, **15**, 193
- King A. R., Ritter H., 1998, *MNRAS*, **293**, L42
- Kippenhahn R., Weigert A., Weiss A., 2012, *Stellar Structure and Evolution*, doi:10.1007/978-3-642-30304-3.
- Kotko I., Lasota J. P., 2012, *A&A*, **545**, A115
- Lasota J.-P., 2001, *New Astron. Rev.*, **45**, 449
- Lasota J. P., Dubus G., Kruk K., 2008, *A&A*, **486**, 523
- Lightman A. P., Eardley D. M., 1974, *ApJ*, **187**, L1
- Lipunova G. V., Malanchev K. L., 2017, *MNRAS*, **468**, 4735
- Lipunova G., Malanchev K., Tsygankov S., Shakura N., Tavleev A., Kolesnikov D., 2022, *MNRAS*, **510**, 1837
- Liu B. F., Meyer-Hofmeister E., 1997, *A&A*, **328**, 243
- Malanchev K. L., Shakura N. I., 2015, *Astronomy Letters*, **41**, 797
- Malanchev K. L., Postnov K. A., Shakura N. I., 2017, *MNRAS*, **464**, 410
- Martin R. G., Nixon C. J., Pringle J. E., Livio M., 2019, *New Astron.*, **70**, 7
- Mescheryakov A. V., Shakura N. I., Suleimanov V. F., 2011, *Astronomy Letters*, **37**, 311
- Meyer F., Meyer-Hofmeister E., 1981, *A&A*, **104**, L10
- Meyer F., Meyer-Hofmeister E., 1982, *A&A*, **106**, 34
- Morrison R., McCammon D., 1983, *ApJ*, **270**, 119
- Paczynski B., 1969, *Acta Astron.*, **19**, 1
- Papaloizou J., Faulkner J., Lin D. N. C., 1983, *MNRAS*, **205**, 487
- Paxton B., Bildsten L., Dotter A., et al., 2011, *ApJS*, **192**, 3
- Rogers F. J., Nayfonov A., 2002, *ApJ*, **576**, 1064
- Scepi N., Lesur G., Dubus G., Flock M., 2018, *A&A*, **609**, A77
- Schwarzschild M., 1958, *Structure and evolution of the stars*.
- Shakura N. I., 1972, *Azh*, **49**, 921
- Shakura N. I., Sunyaev R. A., 1973, *A&A*, **500**, 33
- Shakura N. I., Sunyaev R. A., 1976, *MNRAS*, **175**, 613
- Shakura N. I., Lipunova G. V., Malanchev K. L., et al., 2018, *Accretion flows in astrophysics*. New York, New York, doi:10.1007/978-3-319-93009-1
- Shaviv G., Wehrse R., 1986, *A&A*, **159**, L5
- Smak J., 1982a, *Acta Astron.*, **32**, 199
- Smak J., 1982b, *Communications of the Konkoly Observatory Hungary*, **83**, 195
- Smak J., 1984, *Acta Astron.*, **34**, 161
- Suleimanov V., Meyer F., Meyer-Hofmeister E., 1999, *A&A*, **350**, 63
- Suleimanov V., Meyer F., Meyer-Hofmeister E., 2003, *A&A*, **401**, 1009
- Suleimanov V. F., Lipunova G. V., Shakura N. I., 2007, *Astronomy Reports*, **51**, 549
- Suleimanov V. F., Lipunova G. V., Shakura N. I., 2008a, *A&A*, **491**, 267
- Suleimanov V. F., Lipunova G. V., Shakura N. I., 2008b, *A&A*, **491**, 267
- Tavleev A., Malanchev K., Lipunova G., 2019, in *The Multi-Messenger Astronomy: Gamma-Ray Bursts, Search for Electromagnetic Counterparts to Neutrino Events and Gravitational Waves*. pp 229–233, doi:10.26119/SAO.2019.1.35553
- Tavleev A. S., Lipunova G. V., Malanchev K. L., 2022, in *Astronomy at the Epoch of Multimessenger Studies*. pp 302–303, doi:10.51194/VAK2021.2022.1.1.116
- Tetarenko B. E., Dubus G., Lasota J. P., Heinke C. O., Sivakoff G. R., 2018, *MNRAS*, **480**, 2
- Tuchman Y., Mineshige S., Wheeler J. C., 1990, *ApJ*, **359**, 164
- Walt S. v. d., Colbert S. C., Varoquaux G., 2011, *Computing in Science & Engineering*, **13**, 22
- de Jong J. A., van Paradijs J., Augusteijn T., 1996, *A&A*, **314**, 484

APPENDIX A: IRRADIATION FORMULAS

In this section we write the formulas that describe the irradiation terms in the advanced irradiation scheme (ii), see Sect. 2.4.2.

Assume that the disc is irradiated by external X-rays with spectral

flux $F_X^{\nu}(\nu)$. The angle between the direction of incidence of the X-ray photons and the inward normal to the disc layer surface is θ_0 , while the cosine of this angle we denote as $\zeta_0 = \cos \theta_0$.

The X-ray photons are scattered, absorbed and thermalized in the disc and can serve as additional heating source. The scattering in the medium is assumed to be coherent (Thomson scattering, $\sigma = \sigma_T$), and the opacity coefficient κ^{ν} for X-rays is determined by photoabsorption for a cold gas (Morrison & McCammon 1983).

The mean intensity J_{tot}^{ν} and flux H_{tot}^{ν} of both primary and scattered X-ray photons in the disc at some depth with corresponding τ_{ν} at frequency ν can be found by solving the transfer equation in plane-parallel approximation (Mescheryakov et al. 2011):

$$J_{\text{tot}}^{\nu}(\tau^{\nu}, \nu) = \frac{F_X^{\nu}}{4\pi} \left\{ C^{\nu} \left[e^{-k\tau^{\nu}} + e^{-k(\tau_0^{\nu} - \tau^{\nu})} \right] + (1 - D^{\nu}) \left[e^{-\tau^{\nu}/\zeta_0} + e^{-(\tau_0^{\nu} - \tau^{\nu})/\zeta_0} \right] \right\}, \quad (\text{A1})$$

$$H_{\text{tot}}^{\nu}(\tau^{\nu}, \nu) = F_X^{\nu} \left\{ \frac{k C^{\nu}}{3} \left[e^{-k\tau^{\nu}} - e^{-k(\tau_0^{\nu} - \tau^{\nu})} \right] + \left(\zeta_0 - \frac{D^{\nu}}{3\zeta_0} \right) \left[e^{-\tau^{\nu}/\zeta_0} - e^{-(\tau_0^{\nu} - \tau^{\nu})/\zeta_0} \right] \right\}, \quad (\text{A2})$$

where τ_0^{ν} is the total optical depth of the disc in the vertical direction for X-ray radiation at frequency ν , $\tau^{\nu} = \Sigma(\sigma + \kappa^{\nu})/2$, κ^{ν} is the absorption coefficient for X-ray photons, σ is the scattering coefficient, $k = \sqrt{3(1 - \lambda)}$ and $\lambda = \sigma/(\sigma + \kappa^{\nu})$ is the single-scattering albedo. Formulas for C^{ν} and D^{ν} can be found in Mescheryakov et al. (2011).

The additional heating of the disc by X-ray photons of a given frequency ε^{ν} is proportional to their mean intensity:

$$\varepsilon^{\nu} = 4\pi\rho\kappa^{\nu}J_{\text{tot}}^{\nu}. \quad (\text{A3})$$

The local energy release in the disc through its irradiation by X-ray photons is

$$\varepsilon = \int_0^{\infty} \varepsilon^{\nu} d\nu = 4\pi\rho \int_0^{\infty} \kappa^{\nu} J_{\text{tot}}^{\nu} d\nu. \quad (\text{A4})$$

The flux H_{tot}^{ν} is calculated for all solid angles and it takes into account photons coming into the disc from outside minus those escaping the disc without absorption. Thus, the total heating of the disc from the disc surface to the central plane through its irradiation is

$$Q_{\text{irr}}(z_0) = \int_0^{\infty} H_{\text{tot}}^{\nu}(\tau_{\text{ph}}^{\nu}, \nu) d\nu, \quad (\text{A5})$$

where $\tau_{\text{ph}}^{\nu} = (\sigma + \kappa^{\nu})\Sigma_{\text{ph}}$ is the optical depth of the photosphere layers above the disc surface, Σ_{ph} is the corresponding column density. To find it we can write (cf. (11–12))

$$d\Sigma_{\text{ph}} = -\rho dz = \frac{d\tau}{\kappa_{\text{R}}} \quad (\text{A6})$$

and take the value, evaluated at z_0 , which corresponds to $\tau = 2/3$:

$$\Sigma_{\text{ph}} = \frac{2}{3} \frac{1}{\kappa_{\text{R}}(P_{\text{gas}}(z_0), T(z_0))} = \frac{P_{\text{gas}}(z_0) + P_{\text{rad}}(z_0)}{\omega_{\text{K}}^2 z_0}. \quad (\text{A7})$$

It should be noted that photospheric column density Σ_{ph} is not included into the surface density Σ_0 of the disc when we calculate S-curves.

The irradiation temperature and irradiation parameter can be found from the irradiation flux (A5):

$$Q_{\text{irr}}(z_0) = \sigma_{\text{SB}} T_{\text{irr}}^4 = C_{\text{irr}} \frac{L_X}{4\pi r^2}, \quad (\text{A8})$$

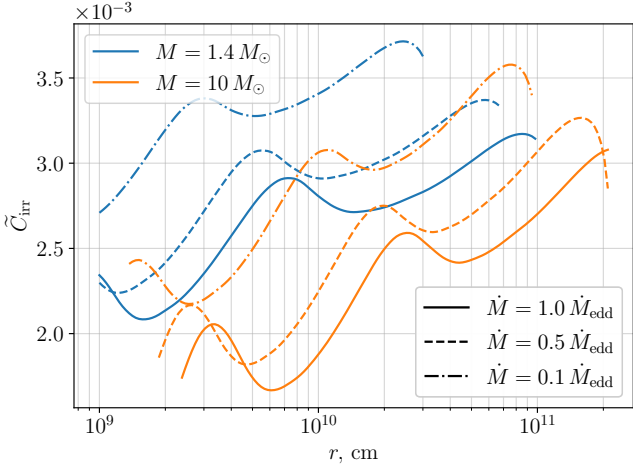


Figure A1. Radial profile of \tilde{C}_{irr} , system parameters and notations are the same as in Fig. 5. It is clearly seen, that this value almost does not change over radius (it changes by a factor of ~ 1.5 by two orders of magnitude along the radius).

where L_X is the X-ray luminosity of the central source.

Notice that ε is the function of Σ , that is, the function of the vertical coordinate z . The total X-ray optical depth is $\tau_0^v = (\sigma + \kappa^v)(\Sigma_0 + 2 \cdot \Sigma_{\text{ph}})$. Therefore, irradiation terms ε and Q_{irr} (as well as T_{irr} and C_{irr}) contain the surface density Σ_0 as an additional free parameter, so the system of equations for the disc vertical structure in irradiation scheme (ii) have two free parameters: z_0 and Σ_0 .

Using (A2), (A5), (A8) and (23), we can obtain exact formula:

$$C_{\text{irr}} = \frac{\int_0^\infty F_X^v \{...\} dv}{\int_0^\infty F_X^v dv} = \int_0^\infty S(v) \{...\} dv, \quad (\text{A9})$$

where expression in $\{...\}$ is the one from the (A2). For a very optically thick disc with $\tau_0^v \gg 1$, exponential terms with τ_0^v tend to zero, and it can be shown that $C_{\text{irr}} \propto \zeta_0$. If additionally we assume $\Sigma_{\text{ph}} = 0$, then $\tau_{\text{ph}}^v = 0$, and we obtain

$$C_{\text{irr}} = \left(1 - \int_0^\infty S(v) \frac{3\lambda}{(1 + k\zeta_0)(3 + 2k)} dv\right) \zeta_0, \quad (\text{A10})$$

or, for single-frequency incoming X-ray photons, $C_{\text{irr}} = (1 - A)\zeta_0$, where the frequency-dependent albedo A is defined following Mescheryakov et al. (2011).

Moreover, one could introduce a notion of a spectrum-integrated albedo:

$$A^* = \int_0^\infty S(v) \frac{3\lambda}{(1 + k\zeta_0)(3 + 2k)} dv. \quad (\text{A11})$$

APPENDIX B: BRIEF CODE DESCRIPTION

The Python 3 code solves the vertical structure equations. It contains several classes which represent the vertical structure for different types of EoS and opacity, temperature gradient and irradiation scheme. Function `StructureChoice()` serves as an interface to initialize the chosen structure type. The code also contains three functions to calculate S-curves, vertical and radial profile of a stationary disc.

Main input parameters of the code are: mass of the central object M , radius r , viscous torque F (or effective temperature T_{eff} or accretion rate \dot{M}), turbulence parameter α and type of the structure (depending on the opacity law, EoS, irradiation scheme, temperature gradient, see the GitHub documentation and the code `help()`). Notice that different chemical composition can be set if tabular opacity and EoS are used (see Sect. 4.2).

If irradiation takes place, there are two cases:

(i) If irradiation is described in terms of T_{irr} or C_{irr} , then the code has one additional input parameter – irradiation temperature T_{irr} or irradiation parameter C_{irr} .

(ii) If irradiation is described through the advanced scheme, the external irradiation flux is given by Eq. (23), and the code has a few more input parameters: the X-ray luminosity of central source L_X ; the spectrum $S(v)$ in form of table values (normalized over the frequency range to unity) or as a Python function; cosine of the incident angle $\cos \theta_0$ as a fixed value or as a fixed value in the brackets in function (see also Eq. (32)):

$$\cos \theta_0 = \frac{z_0}{r} \left(\frac{d \ln z_0}{d \ln r} - 1 \right). \quad (\text{B1})$$

Note that the calculated vertical structure of a disc ring without irradiation differs to minor extent when we use alternative boundary conditions on pressure: (13) and (17). The first boundary condition is implemented as described in section 2.1. The second variant can be engaged in irradiated-disc scheme (ii) with $C_{\text{irr}} = 0$ or $T_{\text{irr}} = 0$.

The free parameter z_0 is found using so-called shooting method. The system is integrated with different values of the free parameter, starting from initial estimation, in order to satisfy the additional condition for flux (14) at the symmetry plane of the disc. In the presence of external irradiation in scheme (i), the only change is the boundary condition for temperature (15). If irradiation is taken into account through the advanced scheme (ii), the system is modified as described in Sect. 2.4.2 and two-parameter (z_0, Σ_0) optimization problem is solved in order to satisfy both the additional boundary conditions (14) and (22).

Code is open-source and available with detailed documentation on GitHub⁶. Scipy (Jones et al. 2019), Numpy (Walt et al. 2011), Matplotlib (Hunter 2007) and Astropy (Astropy Collaboration et al. 2013, 2018) packages are used in the code.

APPENDIX C: VERTICAL STRUCTURE: EXAMPLES

Figure C1 presents examples of the vertical structure for different effective temperatures, which are determined by the accretion rate, at fixed radius $r = 10^{10}$ cm for a case without external irradiation. Shown are the temperature distribution, adiabatic and actual temperature gradients, and the mean number of free electrons per nucleon $e_{\text{free}}^- \equiv 1/\mu_e$. The latter can change from 0 in neutral matter to $(1 + X)/2$ in fully ionized matter, where X is the hydrogen abundance.

The upper panels of Fig. C1 represent stable disc (in hot and cold state), while lower panels show unstable disc with different chemical composition (solar and pure helium). The latter solutions lie on the negative branch on the S-curve, see Sect. 4 and Fig. 8, 10. The unstable state is related to ionization of hydrogen: while the cold disc is neutral ($e_{\text{free}}^- \approx 0$) and hot disc is fully ionized ($e_{\text{free}}^- \approx 0.85$), ionization of unstable disc changes along z between these two limits.

⁶ <https://github.com/AndreyTavleev/DiscVerSt>

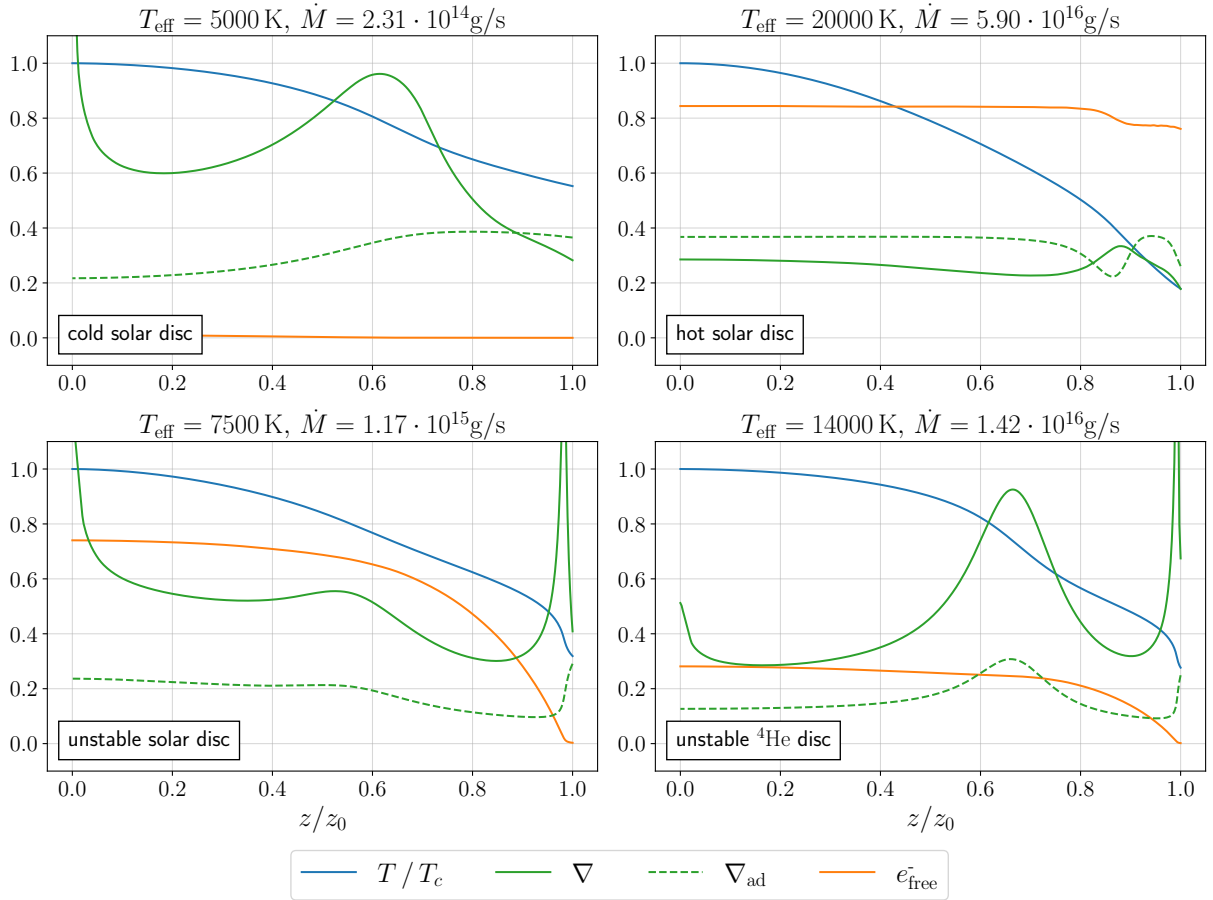


Figure C1. Disc vertical structure for $M = 10 M_{\odot}$, $\alpha = 0.1$, $r = 10^{10}$ cm and tabular opacity for different accretion rates \dot{M} and effective temperatures T_{eff} . Shown are normalized temperature T/T_c , actual temperature gradient ∇ , adiabatic gradient ∇_{ad} , and mean number of free electrons per nucleon. Upper panels are calculated for cold ($T_{\text{eff}} = 5000$ K) and hot ($T_{\text{eff}} = 20000$ K) disc states with solar composition. Lower panels are calculated for unstable disc states with solar and helium composition. There is no convection in the hot disc ($\nabla_{\text{rad}} < \nabla_{\text{ad}}$), while the disc in cold neutral and unstable states is convective.

The disc in cold and unstable state is convective ($\nabla_{\text{rad}} > \nabla_{\text{ad}}$ along the z coordinate), while there is no convection in the hot disc (except for a thin layer near the surface). This happens regardless of the chemical composition: the pure helium disc behaves similarly. The main difference is that instability in helium disc is related to the partial ionization of helium, therefore the temperature of unstable disc ($T_{\text{eff}} \sim 14000$ K) is higher than in that in solar disc ($T_{\text{eff}} \sim 7000$ K). The corresponding S-curves are presented in Sect. 4.2, see Fig. 10.

Figures C2 and C3 show examples of the vertical structure for irradiated disc together with un-irradiated case at two radii $r = 2 \cdot 10^{10}$ and $7 \cdot 10^{10}$ cm. Other system parameters are the same as in Fig. 4: $M = 1.4 M_{\odot}$, $\alpha = 0.1$, $L_X = \eta \dot{M} c^2$, $\eta = 0.1$, $\dot{M} = 10^{18} \text{ g s}^{-1} \approx 0.5 \dot{M}_{\text{edd}}$, the chemical composition is solar. Shown are distributions of mass coordinate Σ , temperature T , flux Q , temperature gradient ∇ and adiabatic temperature gradient ∇_{ad} . Irradiation is taken into account through two methods (i) and (ii), see Sect. 2.4. Irradiation temperature T_{irr} is obtained in advanced method (ii) and serves as input parameter in method (i).

It is clearly seen that at $r = 2 \cdot 10^{10}$ cm the external irradiation with $T_{\text{irr}} = 17330$ K almost does not affect the structure of the disc, whose viscous flux corresponds to $T_{\text{vis}} = 14840$ K. The irradiation does not penetrate deep into the disc and heats only the near-surface

layers, which is seen on the flux dependence in Fig. C2. Energy in the disc is transferred mainly by radiation (see the upper right panel).

At a larger radius $r = 7 \cdot 10^{10}$ cm, the un-irradiated disc with $T_{\text{vis}} = 5800$ K is unstable and fully convective, but irradiation with $T_{\text{irr}} = 9750$ K, affecting the whole disc in the vertical direction, stabilizes the disc structure at a lower surface density and a larger thickness. Without irradiation, opacity κ_R drops in the upper layers by more than two orders. With irradiation, opacity changes with z not more than few times. The convection disappears in the irradiation-stabilized disc.

This paper has been typeset from a \LaTeX file prepared by the author.

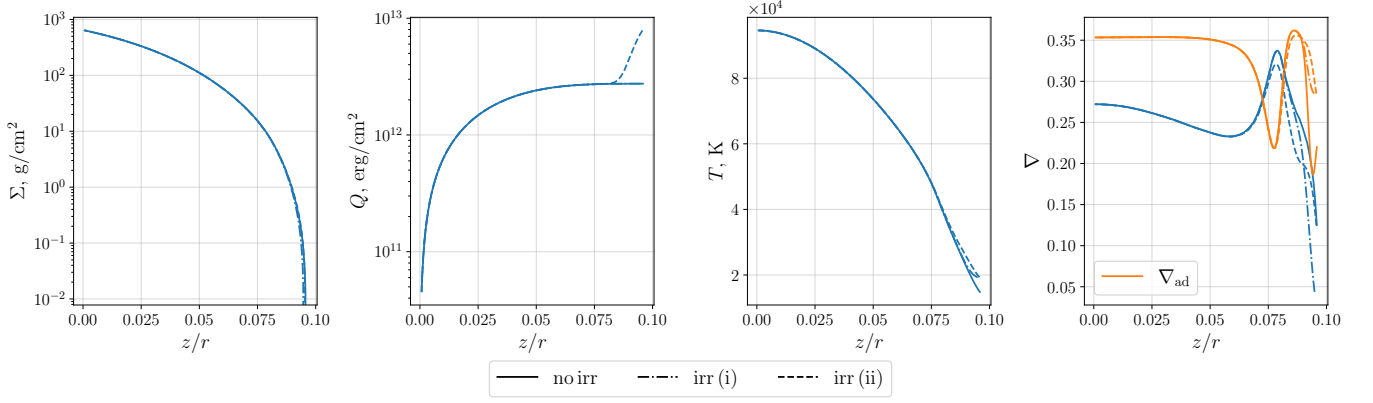


Figure C2. Vertical structure of irradiated disc together with un-irradiated case for $M = 1.4 M_{\odot}$, $\alpha = 0.1$, $r = 2 \cdot 10^{10}$ cm and tabular opacity for accretion rate $\dot{M} = 10^{18}$ g s $^{-1}$. Shown are mass coordinate Σ , temperature T , temperature gradient ∇ , adiabatic gradient ∇_{ad} , and energy flux Q . Irradiation is taken into account through two approaches (i) and (ii), where $L_X = \eta \dot{M} c^2$. Irradiation temperature $T_{\text{irr}} = 17330$ K is obtained from calculations by method (ii) and serves as input parameter in method (i). The corresponding $C_{\text{irr}} = 2.84 \cdot 10^{-4}$.

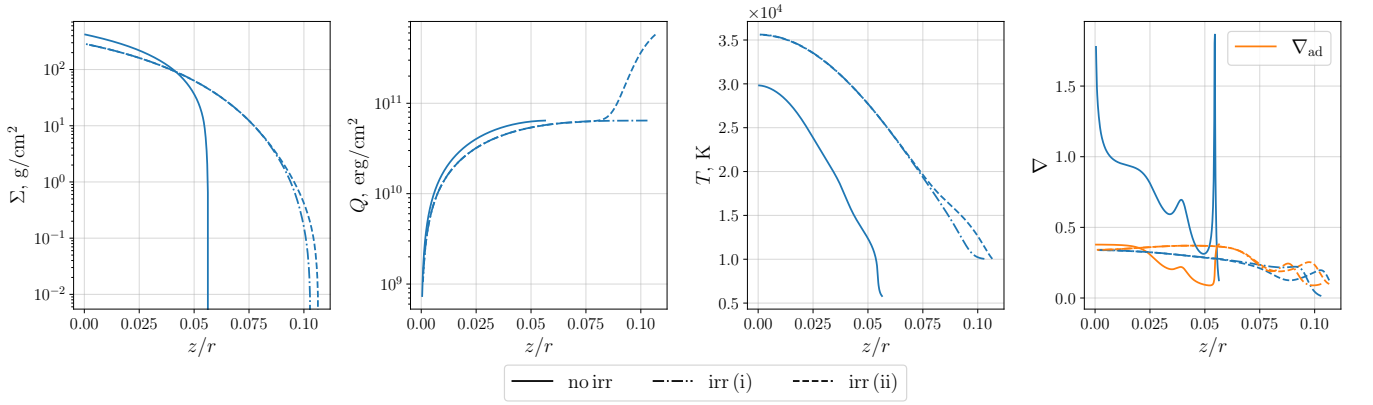


Figure C3. Vertical structure of irradiated disc together with un-irradiated case. System parameters and notations are the same as in Fig. C2, but the radius $r = 7 \cdot 10^{10}$ cm. The obtained $T_{\text{irr}} = 9750$ K, and corresponding $C_{\text{irr}} = 3.5 \cdot 10^{-4}$.